

Rapid Damage Mapping for the 2015 M_w 7.8 Gorkha Earthquake Using Synthetic Aperture Radar Data from COSMO–SkyMed and ALOS-2 Satellites

by Sang-Ho Yun, Kenneth Hudnut, Susan Owen, Frank Webb, Mark Simons, Patrizia Sacco, Eric Gurrola, Gerald Manipon, Cunren Liang, Eric Fielding, Pietro Milillo, Hook Hua, and Alessandro Coletta

ABSTRACT

The 25 April 2015 M_w 7.8 Gorkha earthquake caused more than 8000 fatalities and widespread building damage in central Nepal. The Italian Space Agency's COSMO–SkyMed Synthetic Aperture Radar (SAR) satellite acquired data over Kathmandu area four days after the earthquake and the Japan Aerospace Exploration Agency's Advanced Land Observing Satellite-2 SAR satellite for larger area nine days after the mainshock. We used these radar observations and rapidly produced damage proxy maps (DPMs) derived from temporal changes in Interferometric SAR coherence. Our DPMs were qualitatively validated through comparison with independent damage analyses by the National Geospatial-Intelligence Agency and the United Nations Institute for Training and Research's United Nations Operational Satellite Applications Programme, and based on our own visual inspection of DigitalGlobe's WorldView optical pre- versus postevent imagery. Our maps were quickly released to responding agencies and the public, and used for damage assessment, determining inspection/imaging priorities, and reconnaissance fieldwork.

INTRODUCTION

The M_w 7.8 Gorkha earthquake struck central Nepal on 25 April 2015. The powerful earthquake, which was the strongest to occur in that area since the 1934 Nepal–Bihar earthquake, claimed more than 8000 lives and caused widespread building damage (Government of Nepal, 2015). To assist disaster response efforts, we rapidly produced and released damage proxy maps (DPMs) using Synthetic Aperture Radar (SAR) data from Italian Space Agency's (ASI's) COSMO–SkyMed (CSK) satellites and Japan Aerospace Exploration Agency's (JAXA's) Advanced Land Observing Satellite-2 (ALOS-2), as part of an ongoing collaborative effort between the Jet Propulsion Laboratory (JPL) and the California Institute of Technology, called the Advanced Rapid Imaging and Analysis (ARIA) project. The ARIA team has been developing automated systems to

use remote sensing data for rapid postdisaster products to provide situational awareness. One such product is the DPM. The DPM algorithm is an improved version of comparing two Interferometric SAR (InSAR) coherence maps from before and spanning a disaster event (Yonezawa and Takeuchi, 2001; Fielding *et al.*, 2005; Hoffmann, 2007; Yun *et al.*, 2011). The algorithm was successfully tested with natural disaster events, including the February 2011 M_w 6.3 Christchurch earthquake, 2011 M_w 9.0 Tohoku earthquake and tsunami, and 2013 Super Typhoon Haiyan (National Aeronautics and Space Administration [NASA], 2013; Yun, 2014; Milillo *et al.*, 2015).

Four days after the Gorkha earthquake (29 April), the first postearthquake single frame CSK data were acquired over the Kathmandu area, and within 24 hours of receipt, we produced a DPM that showed areas of potential damage, and released it to the responders and the public (NASA, 2015a). On 2 May 2015, ALOS-2 acquired a postearthquake SAR image, and on 5 May we produced and released DPMs from three consecutive frames of ALOS-2 data (NASA, 2015b). CSK SAR data discovery and ingestion were automatically done by the ARIA system, and InSAR processing and DPM production were manually implemented for this event. Here, we summarize the data used, methods applied, and results compared with independent observations and analyses.

SAR DATA

ASI's CSK mission consists of a constellation of four identical X-band SAR satellites that have been fully operational since 2011. Each satellite runs 14.8125 orbits a day and repeats the same ground track every 16 days, achieving a nominal average revisit time of four days. JAXA's new L-band SAR satellite ALOS-2 was launched in May 2014 and became operational in November 2014, with a revisit time of 14 days. We used three SAR scenes for each frame from these sensors to produce DPMs. See Table 1 for relevant SAR data parameters. For each sensor, the first two scenes form a reference pair and the second and the third scenes form a coseismic pair. We compared the

Table 1
Parameters of Synthetic Aperture Radar (SAR) Data Used

Sensor	Wavelength	Acquisition Date	Imaging Mode	Resolution	Polarization	Orbit	Bperp (m)*
		(yyyy/mm/dd)		(m)		Direction	
CSK	X-band (3.1 cm)	2014/11/16	Stripmap	3	HH	Descending	86
		2014/11/24		3		Descending	0
		2015/04/29		3		Descending	28
ALOS-2	L-band (23.8 cm)	2014/10/04	Stripmap (SM3)	10	HH	Ascending	-198
		2015/02/21		10		Ascending	0
		2015/05/02		10		Ascending	897

CSK, COSMO–SkyMed; ALOS, Advanced Land Observing Satellite.

*The Bperp represents perpendicular baseline with respect to master scenes, which are indicated by 0 m in the Bperp column.

InSAR coherence maps of the reference and coseismic pairs and identified pixels that show significantly increased decorrelation (loss of correlation) in the coseismic pair relative to the reference pair. The ALOS-2 mission has three different beams along a single orbit path with a given stripmap (SM) imaging mode (in this case, path 157 and SM3 mode). Only one of the beams can be used during a single pass of the satellite if in SM mode.

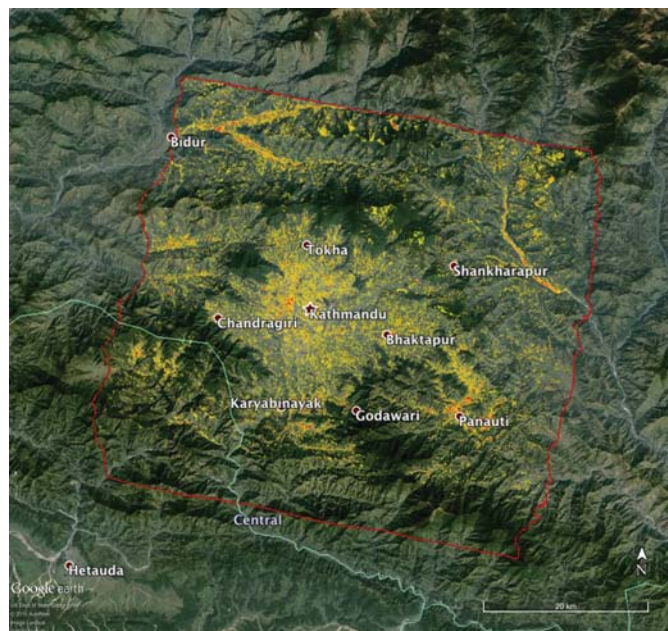
Hours after the earthquake on 25 April, the ARIA team produced a finite-fault model constrained by teleseismic data (JPL, 2015). The fault model indicated that the largest ground surface deformation should be observed near Kathmandu, even though the epicenter of the earthquake was near Gorkha, about 80 km northwest of Kathmandu. Based on the finite-fault model, we issued a recommendation for ALOS-2 data acquisition to JAXA so that the first postearthquake data acquisition over path 157 should be made to cover the Kathmandu area corresponding to the region of maximum expected ground deformation. Two pre-earthquake archived scenes imaged with the same imaging parameters enabled rapid generation of the ALOS-2 DPM of the hardest hit areas, including the capital of Nepal.

DAMAGE PROXY MAP

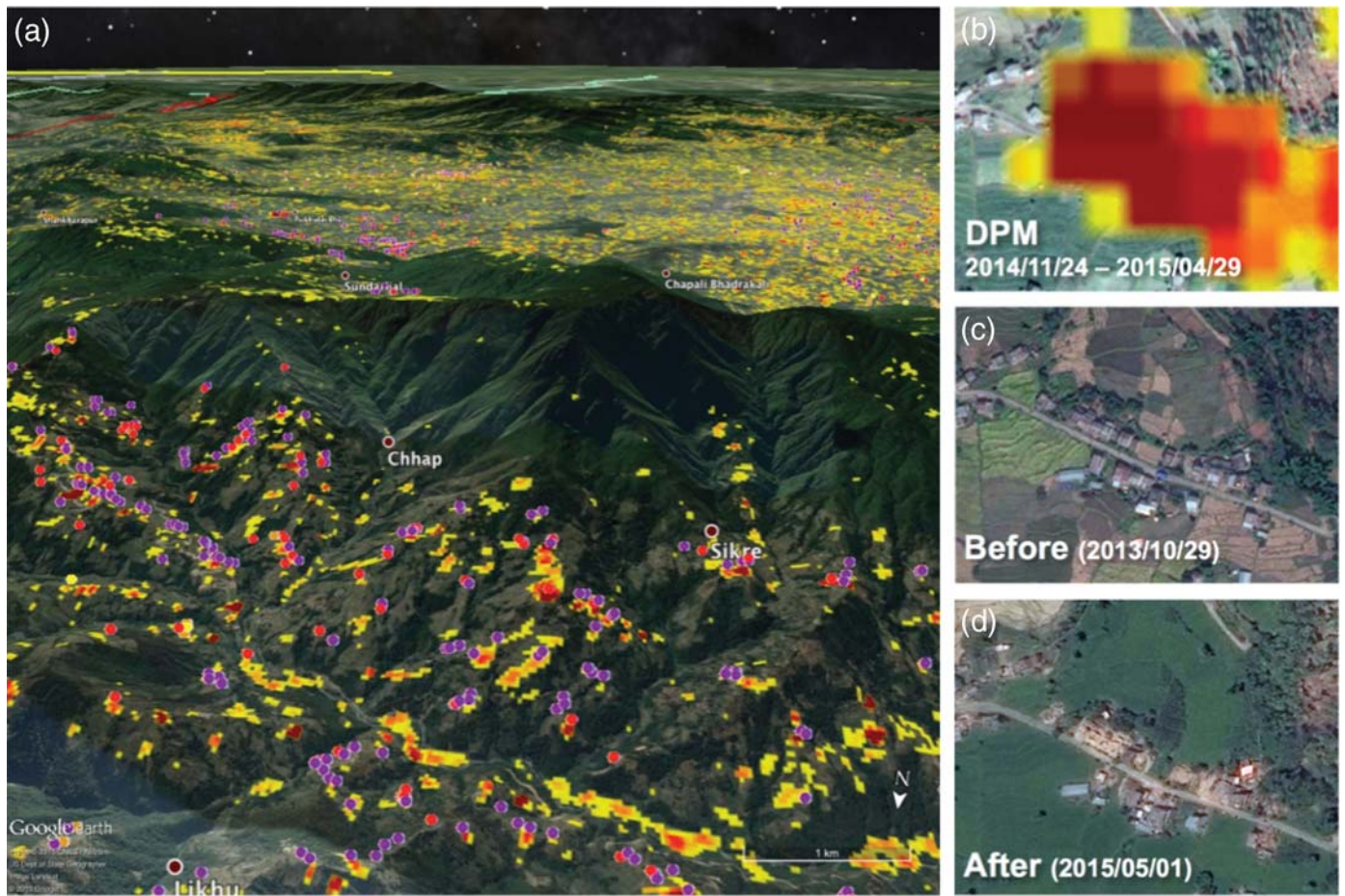
We first started with processing raw CSK data and single-look complex (SLC) images of ALOS-2 using the InSAR Scientific Computing Environment (ISCE) developed at JPL (Rosen *et al.*, 2011) to produce interferometric coherence maps from the reference and coseismic pairs. The coherence maps were estimated over 3×3 pixel windows after topographic phase was removed using the 1-arcsec Shuttle Radar Topography Mission (SRTM) digital elevation model (DEM) (Farr *et al.*, 2007). Resulting coherence pixel values were adjusted to remove estimation bias (Hanssen, 2001; Zebker and Chen, 2005). The coherence maps were registered to each other by calculating dense subpixel offsets with cross correlation on the SAR amplitude images. The calculated relative offset fields were masked to remove outliers and interpolated to register the

coseismic coherence map to the reference coherence map, a process called rubber sheeting (e.g., Yun *et al.*, 2007).

After spatial registration, we applied histogram matching to the resampled coseismic coherence map, such that pixel value statistics of it became identical to that of the reference coherence map. We then took the difference of the coherence maps and applied a color map and transparency mask to produce PNG image files. Combined with geographic bounding box information, the images were compressed into Keyhole Markup language Zipped (KMZ) files for visualization in Google Earth. The DPM pixel boundaries were converted to line segments and merged to produce DPM polygons, and the polygons were stored into Keyhole Markup Language (KML)



▲ **Figure 1.** Damage proxy map (DPM) derived from X-band COSMO–SkyMed (CSK) SAR data and draped on Google Earth. The red bounding box is the boundary of analysis (radar footprint). Yellow to red pixels indicate increasingly more significant potential damage.



▲ **Figure 2.** (a) Blowup and perspective view of the CSK DPM (Fig. 1), showing the detected potential damage in the mountainous areas. The viewing direction is roughly from north to south (Kathmandu is seen over the mountain range). National Geospatial-Intelligence Agency's (NGA's) analysis results are indicated with the red and purple dots, representing severely damaged and collapsed, respectively. (b) Red pixels in the DPM indicating areas of potential damage. (c) Pre- and (d) postearthquake images provided by DigitalGlobe's WorldView satellites. The postearthquake image shows houses along the road devastated by the earthquake.

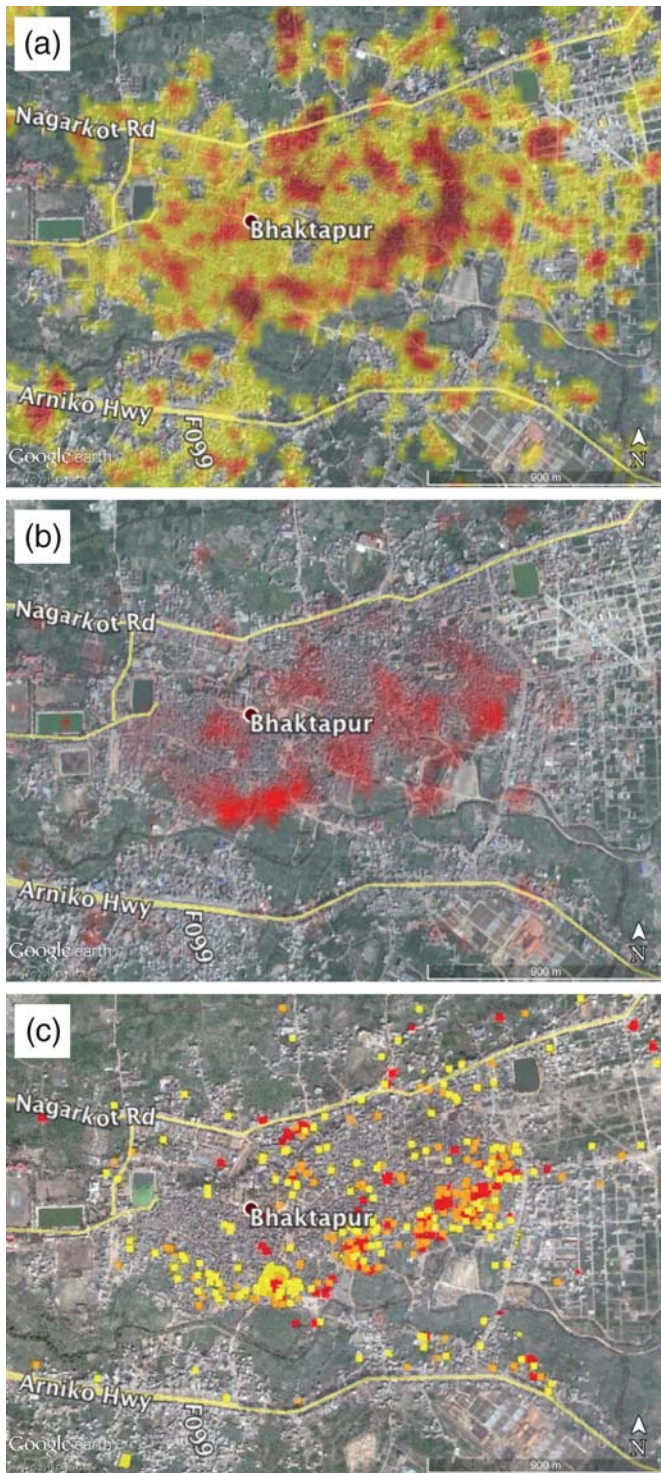
files and Shapefiles for Geographic Information Systems analysis. We also produced GeoTiff files for generic image processing and analysis.

RESULTS

Our first DPM was generated from CSK data (see Table 1) and registered to the SRTM DEM. Figure 1 shows the map view of the CSK DPM draped on Google Earth. The bounding box, morphed to the underlying topography, indicates the extent of CSK image footprint, which covers about 2500 km² (50 × 50 km). The assessment technique is most sensitive to destruction of the built environment. Pixels, corresponding to areas where decorrelation did not significantly increase during the time spanning the earthquake suggesting little to no destruction, are set to be relatively transparent. Increased opacity of the radar image pixels reflects increasing ground and building change or potential damage, with areas in red reflecting the heaviest potential damage. We set the color scale so that the saturated red color represents the top 0.1% of most

decorrelated pixels within the radar footprint. Color variations from yellow to red indicate increasingly more significant change in the area covered by the pixel. Each pixel in the DPM was registered to the SRTM DEM and has a corresponding dimension of about 30 m.

We found, from our qualitative validation, good correlations between the CSK DPM and independent analyses by other groups. The qualitative validation was done by comparison with National Geospatial-Intelligence Agency (NGA) analysis (30 April 2015 preliminary damage assessment product) and the United Nations Operational Satellite Applications Programme (UNOSAT) damage assessment map (released on 30 April 2015), both of which are based on manual visual inspection of high-resolution optical imagery. We overlaid CSK DPM pixels with NGA damage centroid placemarks on Google Earth and observed good spatial correlation between them. Figure 2a shows the CSK DPM in perspective view with the centroid locations of damaged structures identified by the NGA preliminary damage assessment (NGA, 2015a). Many colored pixels in the DPM appear in the same



▲ **Figure 3.** (a) DPM from CSK data showing areas near Bhaktapur, (b) DPM from Advanced Land Observing Satellite-2 (ALOS-2) of the same area, and (c) damage map produced by United Nations Operational Satellite Applications Programme (UNOSAT) based on visual inspection of WorldView-3 images.

locations of the red and purple dots in the NGA's analysis results, revealing damaged structures in small villages in the mountains, often on ridge tops. We also compared the DPM

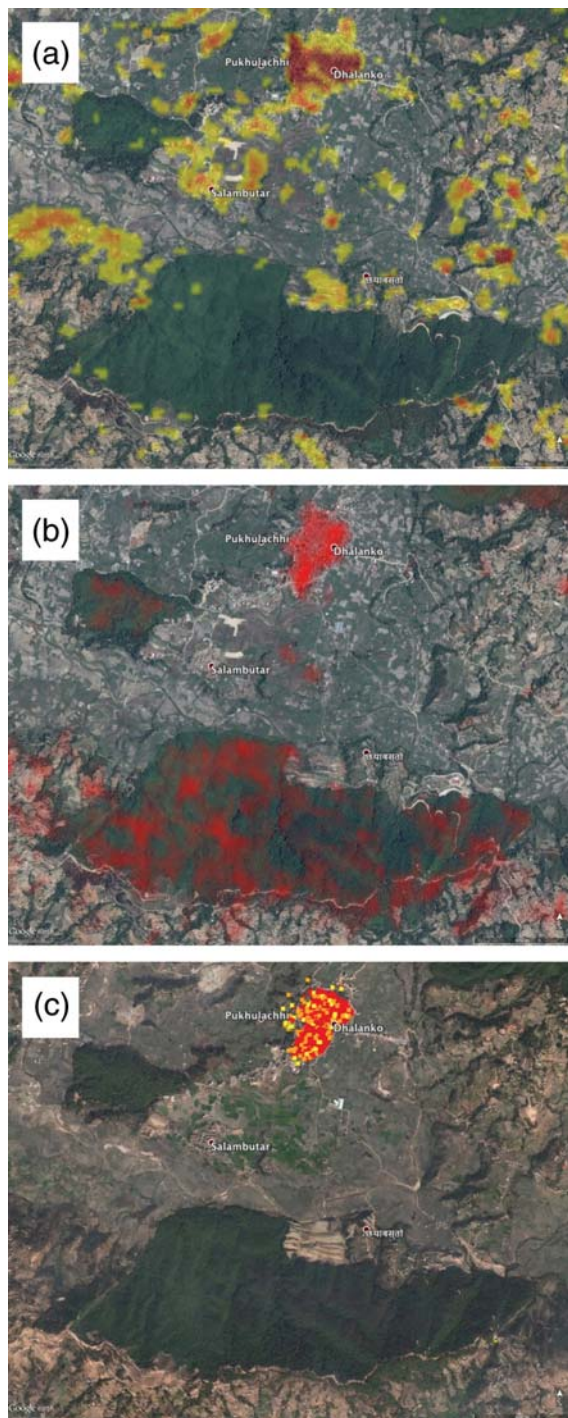
with DigitalGlobe's WorldView images. The DPM estimates correlate with damaged buildings, as shown by the collapsed structures in the "after" image (Fig. 2b–d).

We also observed similarity between the distribution of red pixels in the DPM and independent analysis by UNOSAT that covers Bhaktapur, an ancient city in the east corner of the Kathmandu Valley (Fig. 3) (UNOSAT, 2015). The chain of the detected damaged structures running roughly east to west in the middle is commonly visible in all three figures. The CSK DPM may be prone to false positives. The time span of the coseismic pair is 156 days (Table 1), therefore the DPM may include some apparent "damage" pixels due to any significant ground surface change, such as building construction, which occurred over the winter and early spring. We investigated a couple of red blobs in the DPM using Google Earth time slider and found that new buildings were constructed during the time span. The current version of DPM algorithm cannot distinguish building construction from building collapse. These kinds of false positives should become less frequent in the future when using data that more closely bracket a given disaster. The ALOS-2 DPM (Fig. 3b), of which the time span of the coseismic pair is 70 days, contains fewer false positives in this area. ALOS-2 DPM, however, shows more false positives over vegetated areas (see Fig. 4b).

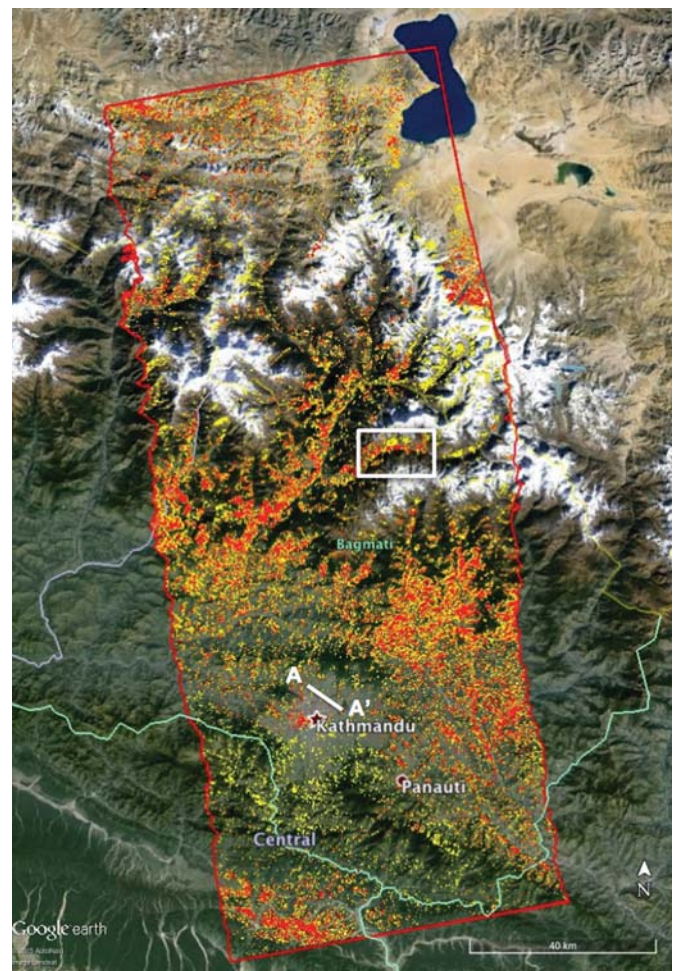
We produced a set of DPMs from ALOS-2 data covering a larger area (70×180 km) (Fig. 5). Three frames (540, 550, and 560) from ascending path 157 were processed individually in the same way as CSK, except that we started from SLCs. The saturated red represents the top 0.01% of decorrelated pixels. Starting from the southernmost frame 540 that includes Kathmandu, we set the color scale so that the distribution of saturated red pixels of ALOS-2 DPM in Kathmandu matches that of CSK DPM. The orange and yellow pixels in Figure 5 represent the top 0.02% and 0.04% of decorrelated pixels, respectively. It was not possible to match the CSK DPM with the distribution of yellow and orange pixels simultaneously with red pixels, because the sensitivity of ALOS-2 DPM is different, so the shape of histograms and the spatial distribution of pixel values are all different. However, we observed similar robust signals that follow the cluster of damage near Bhaktapur (Fig. 3) and Dhalanko (Fig. 4) observed with CSK DPM, ALOS-2 DPM, and UNOSAT analysis. We used the same set of color scales for the other two frames in the north (550 and 560).

When we matched the color scale in urban areas, ALOS-2 produced significantly more "hits" over vegetation in the mountainous areas compared to CSK (see Fig. 4a,b). This is partly due to the L-band (ALOS-2) wavelength being about eight times longer than the X-band (CSK), maintaining good coherence against vegetation in the reference pair. This allows the DPM to show significant vegetation change during the time span of the coseismic pair. For the purpose of structural damage detection, however, the product may need to be filtered through an urban area map or a vegetation mask.

We found a few successful examples of landslide detection in the ALOS-2 DPM in Langtang valley, one of the most



▲ **Figure 4.** (a) DPM from CSK data showing areas including (upper middle) Dhalanko, (b) DPM from ALOS-2 of the same area, and (c) damage map produced by UNOSAT. (a) Note that CSK DPM has fewer false positives over vegetation, whereas (b) ALOS-2 DPM has fewer false positives in the urban areas. The false positives in this ALOS-2 DPM in the mountains may be due to vegetation change in the coseismic pair relative to the reference pair. The CSK radar signal is in X-band, about eight times shorter than that of ALOS-2 (L-band). Thus, CSK data tend to lose coherence much more with vegetation than ALOS-2, causing the reference pair already decorrelated, hence no signal in DPM.



▲ **Figure 5.** DPM derived from ALOS-2 data. The large red rectangle modulated with the topography is the combined radar footprint from three consecutive frames along the ascending track. The small white rectangle indicates the location of Langtang valley (see Fig. 6). The A–A' profile is shown in Figure 8.

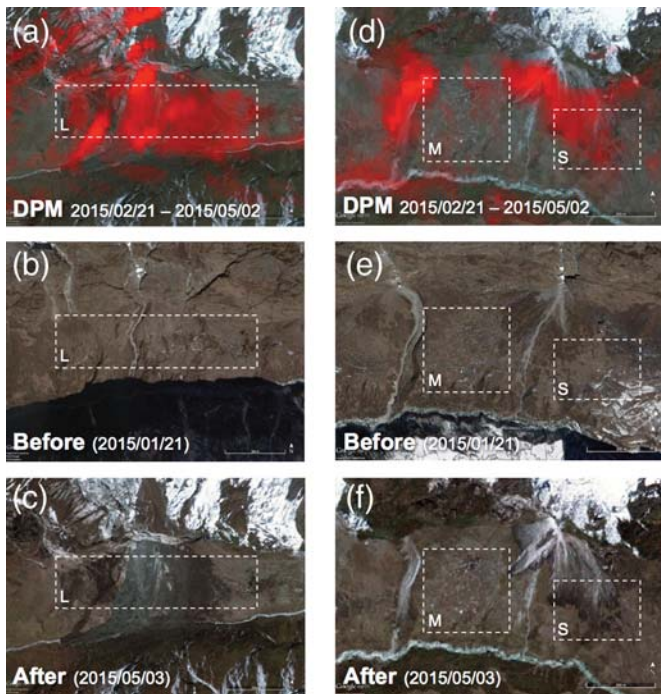
popular trekking destinations in the Himalayas. The earthquake caused rocks and ice to fall and bury almost the entire Langtang village of 55 hotels, guesthouses, and homes, and damaged other villages in the Langtang valley (British Broadcasting Corporation [BBC], 2015; Nepali Times, 2015). Three major landslides were reported to have damaged villages (indicated in Fig. 6) in Langtang Valley (NGA, 2015b; Pacific Disaster Center [PDC], 2015), and we observed that the ALOS-2 DPM roughly delineated the extent of the debris of the reported landslides (Fig. 7).

CONCLUSIONS AND DISCUSSION

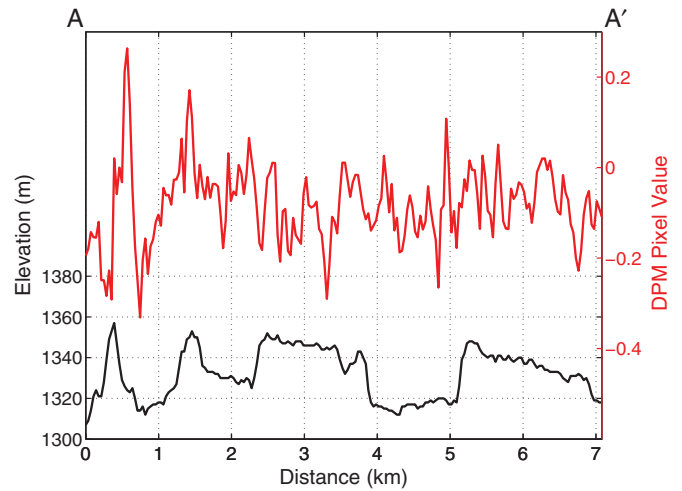
Responding to the 2015 M_w 7.8 Gorkha earthquake, we rapidly produced and publicly released DPMs that highlight areas of potential damage. The DPMs were derived from ASI's CSK and JAXA's ALOS-2 SAR data using our prototype algorithm. Four days after the earthquake, the first postearthquake CSK data



▲ **Figure 6.** Perspective view of Langtang valley with the ALOS-2 DPM (red pixels as shown in Fig. 5) draped on Google Earth. Chyamki, Langtang, Mundu, and Sindum villages were reported to be damaged by induced landslides.



▲ **Figure 7.** Close-up views of (a–c) Langtang village and (d–f) Mundu and Sindum villages, indicated with the white dashed boxes from left to right, (a,d) ALOS-2 DPMs on Google Earth. (b,c,e,f) Pre- and postearthquake pan-sharpened natural color WorldView images, as in NGA’s early analysis (i.e., NGA, 2015b). (c–f) The post-earthquake optical images clearly show the spatial extent of the landslide/avalanche debris, and (a,d) the red pixels in the ALOS-2 DPMs roughly follow the extent of the debris.



▲ **Figure 8.** The profiles of the raw ALOS-2 DPM (red) and the Shuttle Radar Topography Mission (SRTM) digital elevation model (black) along A–A’ in Figure 5. Some correlation between the DPM and the topography is visible in the narrow ridges. Because of the sensitivity of DPM over urban and vegetated areas is different, the profile was selected only within urban area identified with the Global Urban Footprint derived from the German Aerospace Center’s (DLR’s) X-band TerraSAR-X SAR data.

Table 2 Damage Proxy Map (DPM) Users	
Users	What They Are/Were Used for
World Bank	Damage assessment for economic loss
NGA	Determine priority areas for analysis
USGS	Search for land damage and surface rupture
OFDA/USAID	Damage assessment for response on the ground
ICIMOD	Search for land damage, landslides, and river blockage
GEER	Guidance for geotechnical engineer reconnaissance fieldwork
DigitalGlobe	Determine priority areas for high-resolution image acquisition
ESRI	Post on their interface for sharing

NGA, National Geospatial-Intelligence Agency; USGS, U.S. Geological Survey; GEER, Geotechnical Extreme Events Reconnaissance; ESRI, Environmental Systems Research Institute.

were acquired, and we produced a DPM of the Kathmandu area on the following day. The DPM showed good spatial correlation with independent analyses performed by NGA (placemarks in KML file) and UNOSAT (a map in PDF file). The color scale of ALOS-2 DPMs was calibrated using CSK DPM, and the resulting maps correctly delineated the extent of debris from reported landslide/avalanche events in Langtang valley. Our brief investigation suggests potential correlation between the level of dam-

age and topography as was observed in Port-au-Prince after the 2010 M_w 7.0 Haiti earthquake (Hough *et al.*, 2010, 2011). Figure 8 shows the profiles of ALOS-2 DPM before taking a threshold and the SRTM DEM in an urban area north of Kathmandu, masked using the Global Urban Footprint (Esch *et al.*, 2013). The raw DPM pixel values somewhat correlate with narrow ridges but not as much with broad ridges. More in-depth subsequent work will be needed to further explore the effect of topography on the level of damage. The DPMs were downloaded 3198 times in May 2015. Some of the major users and their usage of the DPMs are summarized in Table 2. We continue developing the algorithm and the automated system for more reliable products with reduced latency.

DATA AND RESOURCES

Damage proxy maps (DPMs) were created in KML (with PNG and polygons), GeoTiff, and Shapefile formats and are available to download. Interested readers can obtain the maps from http://aria-share.jpl.nasa.gov/events/20150425-Nepal_EQ/DPM/ (last accessed July 2015). ☒

ACKNOWLEDGMENTS

The COSMO–SkyMed data were made available for disaster response by the Italian Space Agency (ASI). The Advanced Land Observing Satellite-2 (ALOS-2) radar data were made available by the Japan Aerospace Exploration Agency (JAXA) through the Committee on Earth Observation Satellite (CEOS) in support of the response effort. The Global Urban Footprint was provided by German Aerospace Center (DLR) for disaster response. We thank Matthew Gamm and his team with the National Geospatial-Intelligence Agency (NGA), Thomas Esch with DLR, Keiko Saito with the World Bank, Shay Har-Noy, and Andrew Steele with DigitalGlobe, David Saeger with Office of Foreign Disaster Assistance (OFDA)/United States Agency for International Development (USAID), Mir Martin, and Deo Raj Gurung with the International Centre for Integrated Mountain Development (ICIMOD), Jon Pedder with Esri, and Mike Rubel with Planet Labs for supportive coordination and analysis for response. Constructive comments from Susan Hough, Gerald Bawden, and two anonymous reviewers improved the article. This research was supported by the National Aeronautics and Space Administration Applied Sciences/Disasters Program and Advanced Information Systems Technology (AIST) Program, and performed at the Jet Propulsion Laboratory (JPL), California Institute of Technology.

REFERENCES

British Broadcasting Corporation (BBC) (2015). Nepal earthquake: “Worst-affected” village of Langtang, <http://www.bbc.com/news/world-asia-32585356> (last accessed May 2015).

Esch, T., M. Marconcini, A. Felbier, A. Roth, W. Heldens, M. Huber, M. Schwinger, H. Taubenbock, A. Muller, and S. Dech (2013). Urban footprint processor—Fully automated processing chain generating settlement masks from global data of the TanDEM-X mission, *Geosci. Remote Sens. Lett. IEEE* **10**, no. 6, 1617–1621.

Farr, T. G., P. A. Rosen, E. Caro, R. Crippen, R. Duren, S. Hensley, M. Kobrick, M. Paller, E. Rodriguez, L. Roth, *et al.* (2007). The shuttle radar topography mission, *Rev. Geophys.* **45**, doi: [10.1029/2005RG000183](https://doi.org/10.1029/2005RG000183).

Fielding, E. J., M. Talebian, P. A. Rosen, H. Nazari, A. Jackson, M. Ghorashi, and R. Walker (2005). Surface ruptures and building damage of the 2003 Bam, Iran, earthquake mapped by satellite synthetic aperture radar interferometric correlation, *J. Geophys. Res.* **110**, no. B3, B03302.

Government of Nepal (2015). Nepal disaster risk reduction portal, Kathmandu, Nepal, <http://www.drrportal.gov.np/> (last accessed June 2015).

Hanssen, R. (2001). *Radar Interferometry: Data Interpretation and Error Analysis*, Kluwer Academic Publishers, Dordrecht, The Netherlands.

Hoffmann, J. (2007). Mapping damage during the Bam (Iran) earthquake using interferometric coherence, *Int. J. Remote Sens.* **28**, no. 6, 1199–1216.

Hough, S. E., J. R. Altidor, D. Anglade, H. Benz, W. Ellsworth, D. Given, J. Hardebeck, M. G. Janvier, J. Z. Maharrey, Y. Mazabraud, *et al.* (2010). Localized damage associated with topographic amplification during the 12 January 2010 M 7.0 Haiti earthquake, *Nat. Geosci.* **3**, 778–782.

Hough, S. E., A. Yong, J. Altidor, D. Anglade, D. Given, and S. Mildor (2011). Site characterization and site response in Port-au-Prince, Haiti, *Earthq. Spectra* **27**, no. S1, S137–S155.

Jet Propulsion Laboratory (JPL) (2015). NASA/Caltech team images Nepal quake fault rupture, surface movements, <http://photojournal.jpl.nasa.gov/catalog/PIA19384> (last accessed May 2015).

Milillo, P., B. Riel, B. Minchew, S.-H. Yun, M. Simons, and P. Lundgren (2015). On the synergistic use of SAR constellations data exploitation for earth science and natural hazard response, in *Selected Topics in Applied Earth Observations and Remote Sensing*, Vol. PP, 1–6, doi: [10.1109/JSTARS.2015.2465166](https://doi.org/10.1109/JSTARS.2015.2465166)

National Aeronautics and Space Administration (NASA) (2013). *NASA Damage Map Helps in Typhoon Disaster Response*, <http://www.nasa.gov/centers/jpl/news/typhoon20131113.html#.VYEs11VvIkp> (last accessed November 2013).

National Aeronautics and Space Administration (NASA) (2015a). *NASA Aids Response to Nepal Quake*, <http://www.nasa.gov/feature/nasa-aids-response-to-nepal-quake> (last accessed May 2015).

National Aeronautics and Space Administration (NASA) (2015b). *New ALOS-2 Damage Map Assists 2015 Gorkha, Nepal Disaster Response*, <http://www.nasa.gov/jpl/new-alos-2-damage-map-assists-2015-gorkha-nepal-disaster-response> (last accessed May 2015).

National Geospatial-Intelligence Agency (NGA) Integrated Work Group for Readiness, Response and Recovery (IWG-R3) (2015a). *Nepal/Latest NGA Damage Assessment Centroid*, https://ngamaps.geointapps.org/arcgis/rest/services/NEPAL/Latest_NGA_Damage_Assessment_Centroid/MapServer (last accessed April 2015).

National Geospatial-Intelligence Agency (NGA) (2015b). *Nepal: Langtang Valley Landslide*, https://ago-item-storage.s3.amazonaws.com/acb304256251438f87dac519bd56b93e/U_Landslide_Langtang_Valley_Graphics.pdf?AWSAccessKeyId=AKIAJLEZ6UDU5TV4KMBQ&Expires=1443035730&Signature=1ZyikbdTi7nQU9jG9qm5SG7cp4%3D (last accessed May 2015).

Nepali Times (2015). *Langtang Is Gone*, <http://nepalitimes.com/article/nation/langtang-destroyed-in-earthquake,2205> (last accessed May 2015).

Pacific Disaster Center (PDC) (2015). *Nepal 7.8M—Langtang Valley Landslides and Damaged Buildings*, http://www.pdc.org/UserFiles/File/PDC_Nepal_Landslide_Locations_02MAY15.pdf (last accessed May 2015).

Rosen, P. A., G. Sacco, E. Gurroal, and H. Zebker (2011). *InSAR Scientific Computing Environment*, NASA Tech Briefs 39, <http://ntrs.nasa.gov/archive/nasa/casi.ntrs.nasa.gov/20120000494.pdf> (last accessed September 2015).

United Nations Operational Satellite Applications Programme (UNOSAT) (2015). *Damage Assessment of Bhaktapur, Kathmandu Valley, Nepal*, http://unosat-maps.web.cern.ch/unosat-maps/NP/EQ20150425NPL/UNOSAT_A3_Landscape_Bhaktapur_20150430.pdf (last accessed April 2015).

- Yonezawa, C., and S. Takeuchi (2001). Decorrelation of SAR data by urban damages caused by the 1995 Hyogoken-nanbu earthquake, *Int. J. Remote Sens.* **22**, no. 8, 1585–1600.
- Yun, S. (2014). Damage proxy maps from radar satellites, *U.S. Geological Survey Earthquake Science Center Seminars*, Menlo Park, California, 26 February 2014, <http://earthquake.usgs.gov/regional/nca/seminars/2014-02-26/> (last accessed February 2014).
- Yun, S., E. Fielding, M. Simons, P. Rosen, S. Owen, and F. Webb (2011). Damage proxy map of M 6.3 Christchurch earthquake using InSAR coherence, *Fringe Workshop "Advances in the science and applications of SAR interferometry from ESA and 3rd party missions,"* Frascati, Italy, https://earth.esa.int/documents/10174/1567329/Yun_FRINGE2011.pdf (last accessed September 2011).
- Yun, S., H. Zebker, P. Segall, A. Hooper, and M. Poland (2007). Interferogram formation in the presence of complex and large deformation, *Geophys. Res. Lett.* **34**, no. 12, L12305.
- Zebker, H. A., and K. Chen (2005). Accurate estimation of correlation in InSAR observations, *Geosci. Remote Sens. Lett. IEEE* **2**, no. 2, 124–127.

Sang-Ho Yun
Susan Owen
Frank Webb
Eric Gurrola
Gerald Manipon
Cunren Liang
Eric Fielding
*Pietro Milillo*¹
Hook Hua

Jet Propulsion Laboratory
California Institute of Technology
4800 Oak Grove Drive
Pasadena, California 91109 U.S.A.
shyun@jpl.nasa.gov

Kenneth Hudnut
U.S. Geological Survey
525 South Wilson Avenue
Pasadena, California 91106 U.S.A.

Mark Simons
California Institute of Technology
Seismological Laboratory
Pasadena, California 91125 U.S.A.

Patrizia Sacco
Alessandro Coletta
Italian Space Agency (ASI)
Via del Politecnico snc
00133 Rome, Italy

¹ Also at University of Basilicata, Via Nazario Sauro, 85, 85100 Potenza, Italy.